

Showcasing research from National Engineering Research Center for Colloidal Materials, Shandong University, Jinan, China.

Aggregation-induced photodimerization of an alkynylpyrene derivative as a photoresponsive fluorescent ink

By rationally introducing multiple noncovalent interactions into a well-designed amphiphilic alkynylpyrene derivative, an aggregation-induced photochemical reaction has been successfully achieved. This platform can act as a smart luminescent system towards confidential information encryption and decryption by photolithography and inkjet printing techniques.

As featured in:



See Xing-Dong Xu *et al.*,
J. Mater. Chem. C, 2019, 7, 13786.



ROYAL SOCIETY
OF CHEMISTRY

Celebrating
IYPT 2019

rsc.li/materials-c

Registered charity number: 207890



Cite this: *J. Mater. Chem. C*, 2019, 7, 13786

Aggregation-induced photodimerization of an alkynylpyrene derivative as a photoresponsive fluorescent ink†

Junying Zhang, Shao-Xiong Tang, Rong Fu, Xing-Dong Xu * and Shengyu Feng 

Smart luminescent materials can substantially alter their physicochemical properties with various stimuli and thus have long been a point of interest for the development and manufacture of various commodities. In particular, photoresponsive materials have seen much commercial success as sensors and for applications in the paint and coating industry. Herein, we report the design, synthesis, and material processing of a novel alkynylpyrene derivative. The aggregation behavior of this compound can be fine tuned in response to different conditions, such as solvent polarity, concentration, and ratio of good solvents to poor solvents. In addition, the concentration-dependent ^1H NMR spectroscopic study and single crystal structure of the model compound revealed that multiple weak intermolecular interactions might be responsible for the formation of highly ordered aggregates. With the formation of highly ordered aggregates through molecular self-assembly, photodimerization can be realized effectively with 400 nm LED irradiation. Owing to the invisible and controlled printable characteristics of the aggregates and the conversion process of the luminescent material, we have demonstrated that our platform can act as a smart luminescent system towards confidential information encryption and decryption with various high-resolution patterns by photolithography and inkjet-printing techniques. In addition, the inherent molecular packing of the materials allows us to quench the luminescence of the as-printed characters easily upon blue visible light irradiation and realize the irreversible erasure of the luminescence signal for multiple information rewritable processes. As a result, the present luminescent material will find applications in the fields of optical information storage, information security protection, and erase/rewrite systems and provide a proof-of-principle application.

Received 12th July 2019,
Accepted 3rd October 2019

DOI: 10.1039/c9tc03786a

rsc.li/materials-c

Introduction

In the past few decades, stimuli-responsive luminescent materials have gained considerable attention due to their smart behavior.¹ Such smart materials that are capable of undergoing luminescence color and intensity changes in response to physical and chemical stimuli have opened new paths to numerous applications including mechanochromic materials,² temperature sensors,³ pH detectors,⁴ pressure sensors,⁵ anti-counterfeiting materials,⁶ *etc.* So far, a large number of stimuli-responsive luminescent materials including small organic dyes,⁷ polymers,⁸ and luminescent metal-organic frameworks⁹ have been extensively explored in this field. Through controlling their chemical constitutions or

structures in the aggregate state with various stimuli, tunable luminescence signals can be achieved.

Among all the potential external stimulus strategies, light is an ideal trigger since it features high spatio-temporal resolution, minimal invasiveness and easy control of wavelength, intensity, coverage area, and illumination duration.¹⁰ Furthermore, the possibility to tune its wavelength and intensity guarantees a wealth of solutions when photochromic systems are intelligently designed.¹¹ As such, supramolecular control of photochemical reactions has emerged as an important strategy for the construction of smart materials by [2+2] photodimerizations.¹² However, the current scope of supramolecular photochemistry is generally restricted to reactions occurring in the solid state.¹³ Contrary to this situation, the control of the outcome of intermolecular photochemical reactions in homogeneous solutions remains a significant challenge. By introduction of multiple weak interactions, it may be possible to achieve similar topochemical control in solution reactions as is possible in the solid state.

National Engineering Research Center for Colloidal Materials, Key Laboratory of Special Functional Aggregated Materials of Ministry of Education, Shandong University, Jinan, 250100, Shandong, China. E-mail: xuxd@sdu.edu.cn

† Electronic supplementary information (ESI) available: Details of characterization, crystallographic data (CIF) and more measurement data. CCDC 1937449. For ESI and crystallographic data in CIF or other electronic format see DOI: 10.1039/c9tc03786a

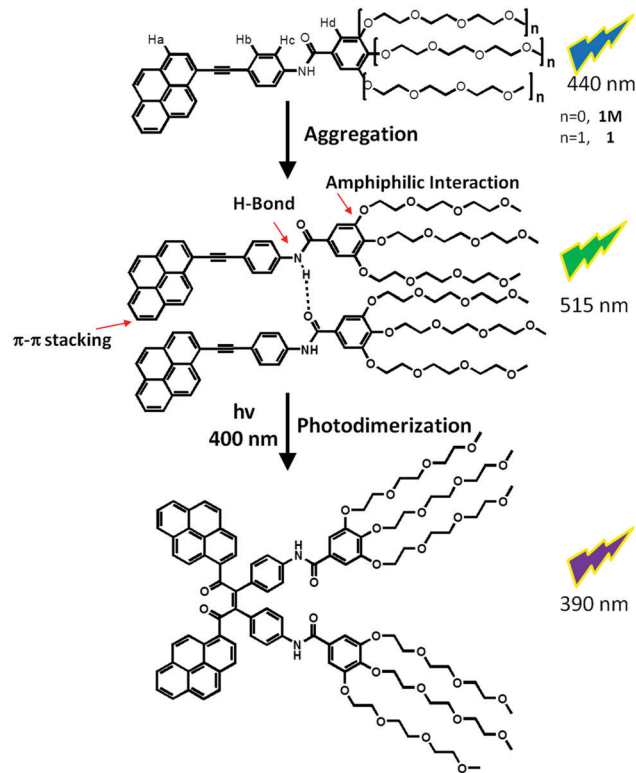
Among the various building blocks used to construct photo-controlled supramolecular materials, pyrene is a well-known conventional organic fluorophore that possesses a number of unique photophysical properties, such as good thermal stability, high fluorescence quantum yield, long fluorescence lifetime, and high polarity dependence of the fine structure of its monomer emission.¹⁴ In addition, the transformation between monomer and excimer with various external stimuli allowed the successful application of pyrenes in optical switches, smart thermosensors, functional photoelectric materials, and information storage media.^{15–17} For example, Kool and co-workers described a photo-switchable DNA-based alkynylpyrene excimer dye that visibly changes fluorescence from green to blue upon UV irradiation.¹⁶ Very recently, we also constructed a fluorescent thermometer based on amphiphilic alkynylpyrene derivatives which exhibits temperature-dependent ratiometric luminescence between red and green and showed their potential applications in temperature gradient distribution and document security.¹⁷ However, it is still a big challenge to realize well-controlled aggregates for a photochemical reaction of a small conjugated pyrene derivative in aqueous solution *via* spontaneous self-assembly.

Based on our previous research results on stimuli-responsive well-controlled aggregates of small organic dyes,¹⁸ we herein designed a novel alkynylpyrene derivative with multiple intermolecular noncovalent interactions. The luminescence behavior can be regulated with an ordered molecule aggregation, which showed blue to green transformation gradually. The photochemical reaction has been successfully developed in the aggregate state, accompanied with purple emission. The effective conversion process showed potential applications in photolithography and inkjet printing, allowing us to develop a platform in which tunable supramolecular nanomaterials can be employed as fluorescent security inks for anti-counterfeiting strategies (Scheme 1).

Results and discussion

The design of the amphiphilic fluorescent compound **1** is based on our previous research results on fluorescent structures.¹⁸ The structure (Scheme 1) employs a conjugated alkynylpyrene fluorophore component, chosen due to its good planarity, strong fluorescence emission characteristics, significant Stokes shift, and sensitive luminescence between the monomer and excimer states. Appended to the fluorophore component is a glycol-based hydrophilic group, which is known for its use in the formation of amphiphilic compounds in the solution phase. The synthesis of an alkynylpyrene complex **1** and **1M** is outlined in Scheme S1 (see ESI†). The resulting molecule was characterized by multiple nuclear NMR spectroscopies (¹H, and ¹³C), and FT-IR and HR-ESI mass spectroscopy and the results were found to be in full agreement with its structure.

With the newly designed alkynylpyrene in hand, the aggregation behaviour of the complex both in solution and on the surface was investigated. Notably, the absorption maximum of the aqueous solution is slightly red-shifted (*ca.* 8 nm) and significantly broadened compared to the absorption spectrum



Scheme 1 Chemical structures and graphical representation of photo-responsive alkynylpyrene derivatives **1** and **1M**.

of **1** in DMSO (1.0×10^{-5} M, Fig. 1a), which can be assigned to the charge-transfer transitions induced by J-aggregation.¹⁹ Interestingly, the alkynylpyrene derivative exhibited solvent-dependent emission properties in solution. For example, the emission color for **1** changed from blue in dichloromethane to green in aqueous solution (Fig. 1b). The Stokes' shifts for **1** consecutively increased, accompanying the disappearance of their vibronic band, with the increase of the solvent polarity. As observed above, the alkynylpyrene derivative showed monomer emission in DMSO and excimer emission in water. So, the aggregation behavior of **1** was also studied in the mixed solvent of DMSO and water. As shown in Fig. 1c and Fig S2 in the ESI,† with the increasing water fraction, an obvious decrease of the high-energy emission intensity was observed. For example, when the water content was increased to 90%, the emission intensity value of **1** at 440 nm decreased approximately 100-fold compared to the starting value. At the same time, excimer emission at 505 nm was observed due to the aggregation of **1** induced by the decrease of solubility. These spectral changes are consistent with the formation of head-to-tail type aggregates with a slip-stacked geometry according to the previous report.

Furthermore, concentration-dependent ¹H NMR spectroscopic studies of **1** in CDCl₃ were performed to probe the driving forces for the aggregation process (Fig. 2). It was found that the resonance of the protons in the aromatic unit displayed an obvious upfield shift upon increasing the concentration (*e.g.*, $\Delta\delta = 0.05$ ppm for H_a, 0.03 ppm for H_b, 0.27 ppm for H_c, and 0.04 ppm for H_d from 1.0×10^{-4} M to 1.0×10^{-3} M),

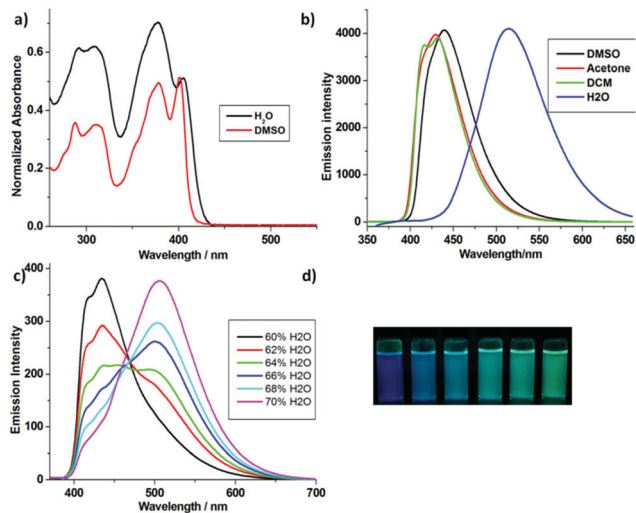


Fig. 1 (a) Normalized UV/Vis spectra of **1** in DMSO and in aqueous solution (1.0×10^{-5} M); (b) fluorescence emission spectra of **1** in different solvents (1.0×10^{-5} M, $\lambda_{\text{ex}} = 340$ nm); (c) fluorescence emission spectra of **1** in DMSO/H₂O mixtures with different DMSO fractions at a fixed concentration (1.0×10^{-5} M, $\lambda_{\text{ex}} = 340$ nm); (d) photoimages of the luminescent color changes of **1** with different DMSO/H₂O ratios (left 70% DMSO, right 60% DMSO) under a 365 nm handheld UV lamp.

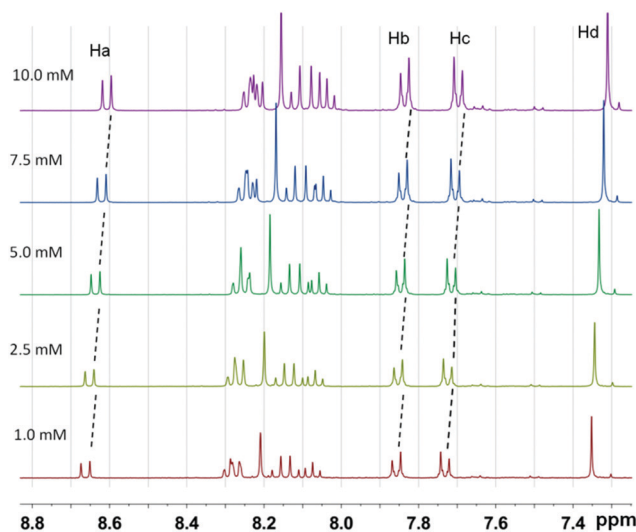


Fig. 2 Region of the ¹H NMR spectrum (400 MHz, CDCl₃, 298 K) of compound **1** at different concentrations.

indicating the existence of π - π stacking interactions during the formation of a supramolecular aggregate. To further corroborate the mechanism of aggregate formation, the Fourier transform infrared (FT-IR) spectrum of the corresponding aggregate was recorded (Fig. S3, ESI[†]). The N-H band centered at 3319 cm^{-1} is characteristic of N-H functions involved in hydrogen bonding interaction.²⁰ The amide I band at 1669 cm^{-1} and the C=O stretching band at 1586 cm^{-1} show evidence for the hydrogen bonding network.

To further understand the packing property of the alkynyl-pyrene derivative in the aggregate state, single crystals of the

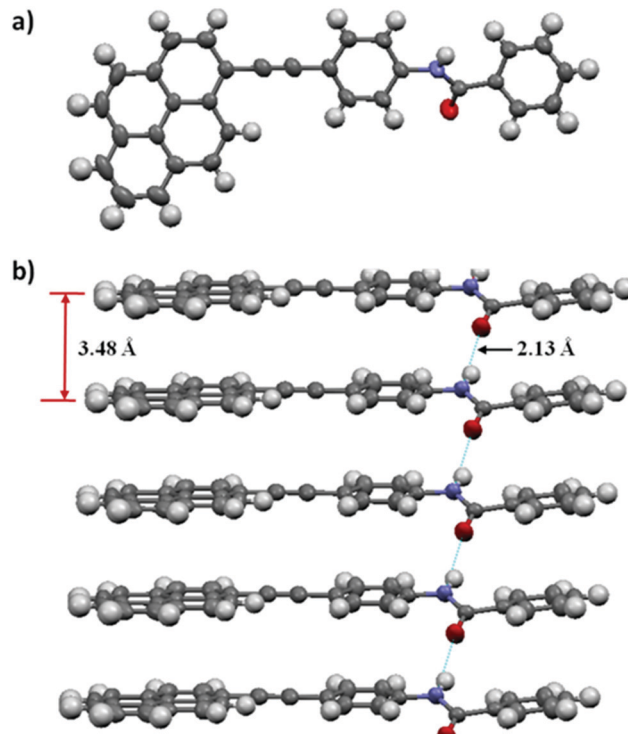


Fig. 3 (a) X-ray crystal structure of a model compound **1M**, and (b) the packing diagram of compound **1M** from side view.

model compound **1M** were grown by slow vapor evaporation of the precursor in solution (CH₂Cl₂/MeOH, 1:1) at ambient temperature for 2–3 days. An ORTEP of compound **1M** (Fig. 3) showed that all of the carbon atoms lay in approximately the same plane. The packing pattern of compound **1M** in the solid state was also investigated. As shown in Fig. 3b, the pyrene rings of two adjacent molecules are stacked in a parallel pattern and the distance between the nearest two pyrene rings in the adjacent molecules was approximately 3.48 Å, which indicates the typical π - π interactions between such molecules in the crystalline state. N-H...O hydrogen bonds with a distance of 2.13 Å are formed between the two neighbouring amide groups. These findings suggest that multiple weak intermolecular interactions may exist in the crystals, which are responsible for the formation of highly ordered aggregates through molecular self-assembly. The identity of the aggregate (mostly in the form of oligomers) was also supported by electrospray ionization mass spectrometry (ESI-MS) studies of **1M** (Fig. S8, ESI[†]), in which the presence of dimeric and trimeric species ($[\text{M}_2 + \text{Na}]^+$ and $[\text{M}_3 + \text{Na}]^+$) apart from monomeric species ($[\text{M} + \text{H}]^+$) was observed. From these results, we infer that the formation of molecular aggregates can be achieved in conjunction with multiple weak interactions including π - π interaction, hydrogen bonding and other weaker interactions.

The nature of multiple intermolecular noncovalent interactions from compound **1** stimulated us to investigate its self-assembly behavior in aqueous solution by using scanning electron microscopy (SEM). As demonstrated in Fig. 4a, the self-assembled amphiphilic derivative **1** exhibits a spherical morphology with a

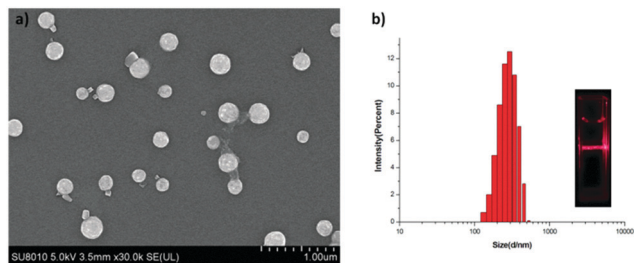


Fig. 4 (a) SEM image of **1** prepared in a DMSO/H₂O mixture (v/v 1 : 99). Scale bar: 1.0 μm; (b) DLS data of the nanospheres self-assembled from compound **1** (1.0×10^{-3} M) with an inset showing the Tyndall effect of compound **1**.

diameter range of 150–300 nm. In addition, the same solution of compound **1** showed clear evidence of the Tyndall effect (inset in Fig. 4b), demonstrating the formation of nanoscale aggregates. Dynamic laser scattering (DLS) examination reveals that the nanospheres have a narrow size distribution, showing an average diameter of 200 nm at a scattering angle of 90° (Fig. 4b).

In general, photochemical [2+2] reactions between two unsaturated bonds will occur when they are arranged in an approximately parallel fashion and are separated by less than 4.2 Å.²¹ Based on the above mentioned research and analysis, the alkynylpyrene derivative **1** in the aggregate state will be an ideal candidate for photodimerization. To investigate the photoreactivity of **1**, a sample of the compound was dissolved in aqueous solution and exposed to a 400 nm light source for irradiation. The excimer emission band at around 515 nm present before irradiation immediately decreased and almost disappeared after 10 seconds (Fig. 5b). Simultaneously, new bands appeared at 380 and 405 nm, which correspond to the emission bands of free pyrene. Furthermore, the isosbestic point at 445 nm was indicative of the selective photodimerization

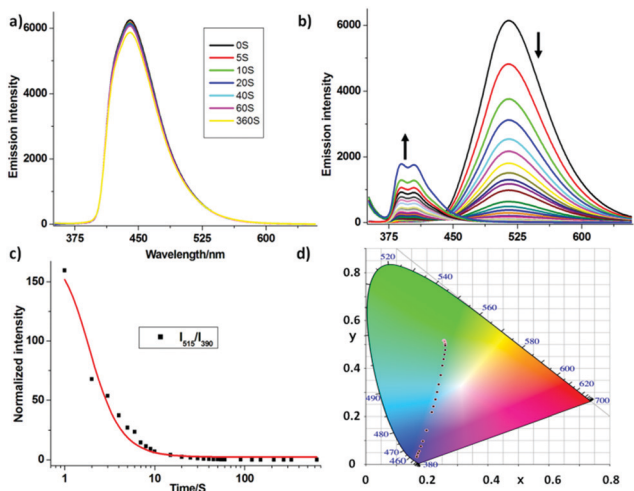


Fig. 5 (a) Emission spectra of alkynylpyrene derivative **1** in DMSO solution over 6 min upon exposure to 400 nm LED light; (b) emission spectra of alkynylpyrene derivative **1** in aqueous solution over 10 min upon exposure to 400 nm LED light; (c) time dependence of the ratio of fluorescence intensity ($I_{515\text{nm}}/I_{390\text{nm}}$) of **1**; (d) CIE chromaticity diagram showing the time dependence of the (x, y) color coordinates of **1**.

reaction between the two unsaturated bonds, which was similar to Kool and coworkers' first report.¹⁶ The transition ratio is 84.0% after 10 s irradiation, 95.2% after 30 s irradiation, and 98.7% after 60 s irradiation upon fluorescence quenching at 515 nm, showing high conversion efficiency. Fig. 5d shows the color change of the luminescence in the Commission Internationale de L'Eclairage (CIE) 1931 coordinates chromaticity diagram with different exposure times. As observed from the CIE coordinates, the coordinates shift from (0.255, 0.517) to (0.166, 0.032), which agrees well with the change in emission spectra and a colour change from green to nearly purple can be seen. Surprisingly, the photochemical reaction did not give the expected dimeric complex in a pure DMSO solution with the same concentration, indicating the importance of ordered molecular packing.

Finally, we have demonstrated the emission patterning by using the phenomenon of photoinduced emission color change, as this is often useful in high-level information storage and security protection applications. Fig. 6 shows that a blue LED (with wavelengths typically at 400 nm) could be used as a pen to write symbols freehand on a filter paper fabricated by drop-casting an aqueous solution of the alkynylpyrene derivative **1**. The regions exposed to the laser beam turned colorless within 60 seconds due to the photochemical reaction of alkynylpyrene, while the unexposed area retained the original excimer emission color of **1**, producing a pattern with sufficient contrast to be observed with the naked eye. Fig. 6 shows the fluorescence images of the papers after irradiation. The characters were clearly recognizable for the irradiated film after irradiation, whereas the pattern was scarcely recognizable before irradiation. The media showed high resolution and good stability under office light conditions, making the system suitable for application in photolithography patterns.

Inkjet printing is a cost effective, readily accessible, high throughput solution processing method for the deposition and incorporation of functional materials onto paper substrates. To demonstrate the behaviour of alkynylpyrene derivative-based fluorescent hydrochromes in this medium, pristine inks comprised of 0.01 mM aqueous solution of the amphiphilic fluorophore were used to fill a conventional inkjet printer cartridge. Images of a brief introduction of Shandong University and a complicated bamboo pattern were then printed on a conventional non-fluorescent A4-sized printer paper (Fig. 7). When visualized under irradiation with 365 nm light, the inkjet printed design exhibited bright fluorescence emission, which visually approximated the chromatic behavior of the previously described compound **1** processed paper.

Benefiting from the good photochemical luminescence behaviors, the assembly could serve as a photoerasable fluorescence ink. In a typical test, some characters were written with the aqueous solution of alkynylpyrene derivative **1** as ink on ordinary white paper, these characters emitted bright green fluorescence upon exposure to UV light at 365 nm after being dried in air (Fig. 8). When irradiated with blue light (400 nm), the characters disappeared within 1 minute. Interestingly, the erased papers can be rewritten multiple times without loss in resolution. These photoerasable properties will enable the application of

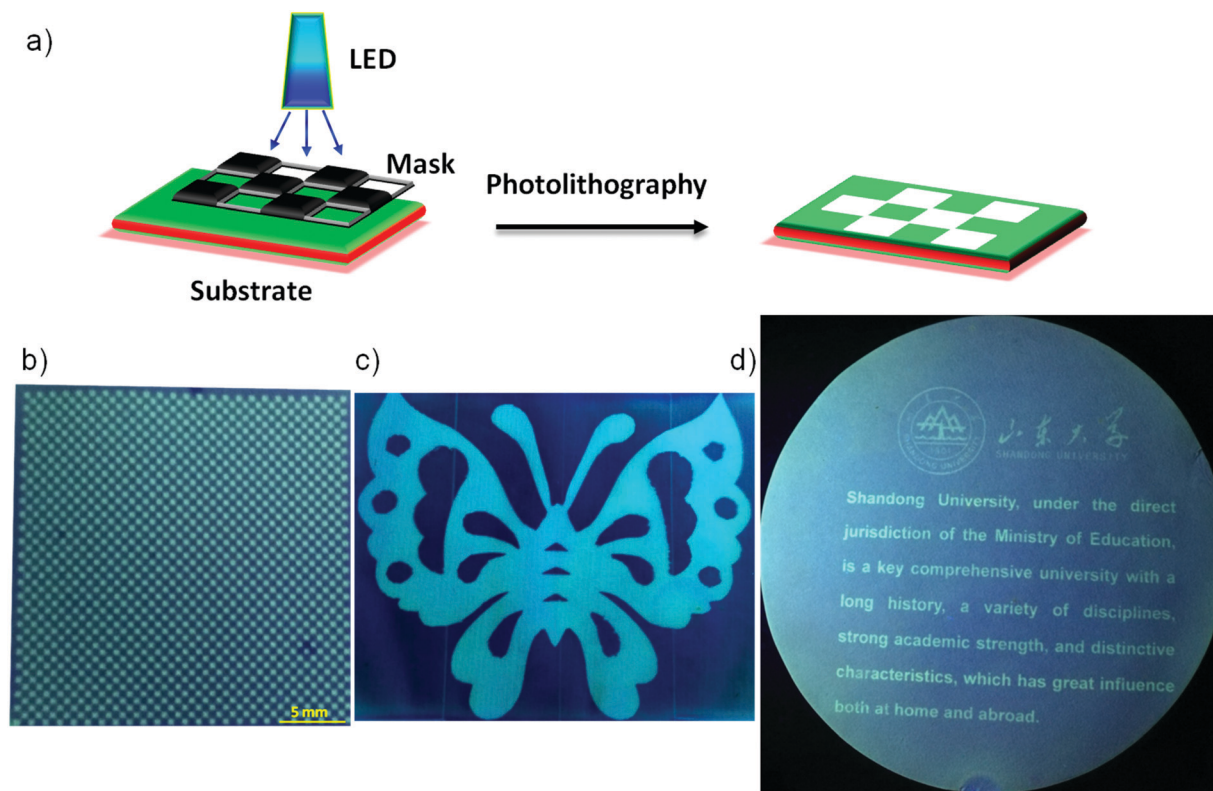


Fig. 6 (a) Schematic illustration of **1** for photolithography upon 400 nm LED irradiation with a photomask which bears patterns that will be printed onto a substrate; sample photographs of (b) a square photomask, (c) butterfly pattern and (d) brief introduction of Shandong University.

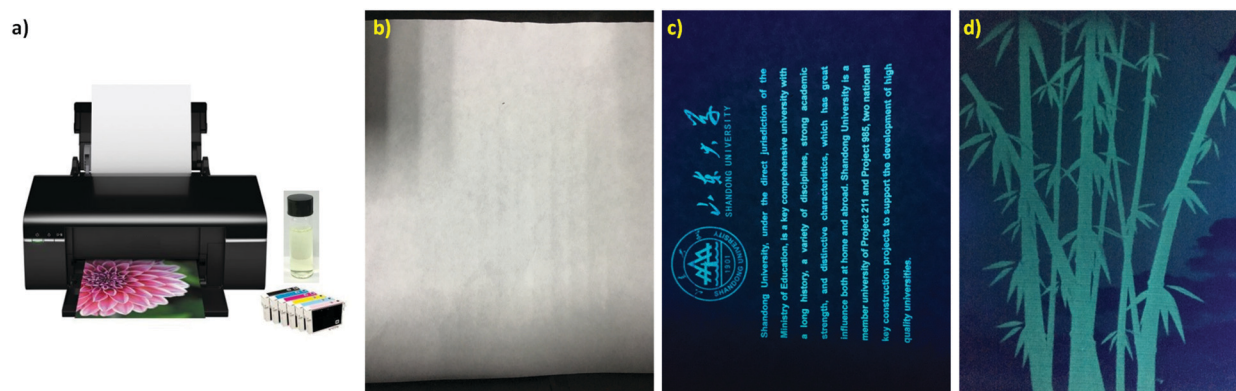


Fig. 7 Luminescent patterns from alkynylpyrene derivative **1** via inkjet printing. (a) Schematic illustrations of the patterning process from a colorless aqueous solution of **1**; digital images of the printed brief introduction of Shandong University on a commercial parchment paper under (b) ambient light and (c) a 365 nm UV lamp; (d) a printed complicated bamboo pattern under irradiation with a 365 nm UV lamp.

the aggregate as a novel anticounterfeiting material in which the information and the state could be effectively written, concealed, read out, and permanently erased by simply alternating the irradiation with UV and visible blue light.

Experimental

General

All reagents and solvents were purchased from commercial sources. THF was distilled from sodium; *i*-Pr₂NH was dried

from potassium hydroxide. All reactions were performed in standard glassware under an inert N₂ atmosphere. Compounds **S0** and **S1** were prepared according to the reported procedure.²² Analytical thin-layer chromatography (TLC) was performed on aluminum sheets, precoated with silica gel 60-F254. Deuterated solvents (Cambridge Isotope Laboratories) for NMR spectroscopic analyses were used as received. ¹H NMR and ¹³C NMR spectra were recorded on a Bruker 400 MHz Spectrometer at 298 K. The ¹H and ¹³C NMR chemical shifts are reported relative to the residual solvent signals. Coupling constants (*J*)

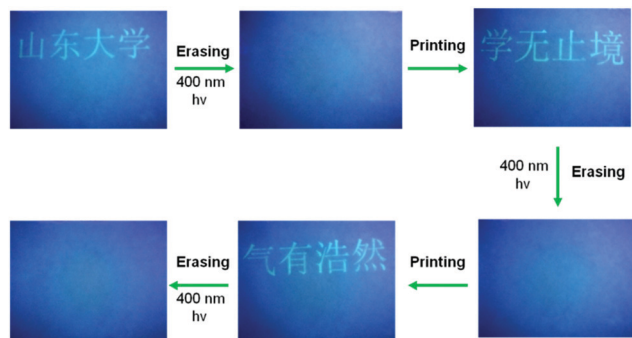


Fig. 8 Photographs of fluorescent inkjet printing-based paper depicting fluorescence erasure before and after being exposed to 400 nm LED under 365 nm irradiation and their rewritable properties.

are denoted in Hz and chemical shifts (d) in ppm. Multiplicities are denoted as follows: s = singlet, d = doublet, m = multiplet. High resolution electrospray ionization (HR-ESI) mass spectral analyses were performed using an AgilentQ-TOF6510. The UV-visible absorption spectra were recorded using a TU-1901 double beam UV-vis spectrophotometer as powders. The fluorescence spectra of the samples were measured using a Hitachi F-7000 fluorescence spectrophotometer using a monochromated Xe lamp as an excitation source. Samples for absorption and emission measurements were placed in 1 cm × 1 cm quartz cuvettes; all the tests were carried out at room temperature if not mentioned. Single crystal X-ray crystallographic analyses were performed using a Bruker Xcalibur ECCD system with graphite-monochromated Mo K α radiation ($\lambda = 0.71073$ Å). Cell parameters were obtained by global refinement of the positions of all collected reflections. Intensities were corrected for Lorentz and polarization effects and empirical absorption. The structures were solved by direct methods and refined by full-matrix least squares on F^2 . The X-ray crystallographic files, in CIF format, are available from the Cambridge Crystallographic Data Centre on quoting the deposition numbers CCDC 1937449 for **1M**.† SEM images were obtained using an S-4800 (Hitachi Ltd) with an accelerating voltage of 1.0 kV or 10.0 kV. Samples were prepared by dropping a dilute solution onto a silicon wafer.

General procedure for the synthesis of compounds **1** and **1M**

A 100 mL Schlenk flask was charged with 1-bromopyrene, the precursors **S0** or **S1**, tetrakis(triphenylphosphine)palladium (10 mol%) and cuprous iodide (5 mol%), degassed, and back-filled three times with N₂. Diisopropylamine and dried THF were introduced into the reaction flask using a syringe. The reaction was stirred under an inert atmosphere at 70 °C for about 24 h. The solvent was removed by evaporation on a rotary evaporator. The residue was purified by column chromatography on silica gel (dichloromethane/methanol = 99:1) to give **1** or **1M** in a reasonable yield.

Compound 1M. Pale yellow solid. Yield: 72.4%. $R_f = 0.51$ (dichloromethane/petroleum ether 2:1); ¹H NMR (DMSO-*d*₆, 400 MHz): δ = 10.50 (s, 1H), 8.65 (d, $J = 12.0$ Hz, 1H), 8.41–8.32 (m, 4H), 8.28–8.22 (m, 3H), 8.16–8.13 (m, 1H),

7.99 (d, $J = 8.0$ Hz, 2H), 7.97 (d, $J = 8.0$ Hz, 2H), 7.79 (d, $J = 8.0$ Hz, 2H), 7.63–7.55 (m, 3H); ¹³C NMR (DMSO-*d*₆, 100 MHz): δ = 166.28, 140.38, 135.25, 132.64, 132.25, 131.46, 131.29, 131.02, 129.98, 129.28, 128.94, 128.78, 128.23, 123.93, 124.19, 125.38, 125.45, 126.41, 126.46, 127.25, 127.74, 117.52, 117.67, 120.72, 96.03, 88.18 ppm; HR-ESI-MS: m/z calcd for C₃₁H₂₀NO: 422.1545 [M + H]⁺; found: 422.1500; C₆₂H₃₈N₂NaO₂: 865.2831 [2M + Na]⁺; found: 865.2712; C₉₃H₅₇N₃NaO₃: 1286.4298 [3M + Na]⁺; found: 1286.4052.

Compound 1. Pale yellow oil. Yield: 79.8%. $R_f = 0.60$ (dichloromethane/petroleum ether 3:1); ¹H NMR (CDCl₃, 400 MHz): δ = 8.68 (d, $J = 8.0$ Hz, 1H), 8.44 (s, 1H), 8.25–8.19 (m, 4H), 8.15–8.02 (m, 4H), 7.79 (d, $J = 8.0$ Hz, 2H), 7.72 (d, $J = 8.0$ Hz, 2H), 7.28 (s, 2H), 4.28–4.24 (m, 6H), 3.88–3.80 (m, 6H), 3.75–3.63 (m, 18H), 3.56–3.52 (m, 6H), 3.38 (s, 3H), 3.34 (s, 6H); ¹³C NMR (CDCl₃, 100 MHz): δ = 165.46, 152.56, 142.08, 138.65, 132.40, 131.79, 131.25, 131.13, 131.08, 129.85, 129.52, 128.27, 128.06, 127.24, 126.20, 125.56, 125.51, 124.52, 124.49, 124.33, 120.12, 118.99, 117.93, 107.98, 95.12, 88.31, 71.91, 71.86, 70.66, 70.64, 70.58, 70.55, 70.50, 70.40, 69.80, 69.25, 58.92 ppm; HR-ESI-MS: m/z calcd for C₅₂H₆₂NO₁₃: 908.4221 [M + H]⁺; found: 908.4053; C₅₂H₆₁NNaO₁₃: 930.4041 [M + Na]⁺; found: 930.3886.

Conclusions

In summary, by rationally introducing multiple intermolecular noncovalent interactions into a well designed amphiphilic alkynylpyrene derivative **1**, an aggregation-induced photochemical reaction has been successfully achieved in the system. Treated under different conditions, such as solvent polarity, concentration, and ratio of good solvents to poor solvents, the aggregation behavior of this compound can be fine tuned with emission color transformation from blue to green. With the formation of highly ordered aggregates through molecular self-assembly, photodimerization can be realized effectively with 400 nm LED irradiation. Owing to the invisible and controlled printable characteristic of the aggregate and the conversion process of the luminescent materials, we have demonstrated that our platform can act as a smart luminescent system towards confidential information encryption and decryption with various high-resolution patterns by photolithography and inkjet-printing techniques, which protect the recorded confidential information from general decryption methods. Corresponding to the previous reports,²³ the anti-counterfeiting technology developed here not only possesses highly advanced anti-counterfeit effect but is also user-friendly and convenient to recognize. In addition, the inherent molecular packing of the materials allows us to quench the luminescence of the as-printed characters easily upon visible light irradiation and realize irreversible erasure of the luminescence signal for multiple information rewritable processes. As a result, the present luminescent materials will provide a platform in the fields of optical information storage, information anti-counterfeiting, and erase/rewrite media.

Conflicts of interest

There are no conflicts to declare.

Acknowledgements

This work was supported by the National Natural Science Foundation of China (Grant No. 21602124), the Natural Science Foundation of Shandong Province (Grant No. ZR2016BQ11), and the Young Scholars Program of Shandong University (2018WLJH40 and 2016TB012).

Notes and references

- (a) X.-Y. Hu, T. Xiao, C. Lin, F. Huang and L. Wang, *Acc. Chem. Res.*, 2014, **47**, 2041–2051; (b) M. Zhang, X. Yan, F. Huang, Z. Niu and H. W. Gibson, *Acc. Chem. Res.*, 2014, **47**, 1995–2005; (c) Z. Gao, Y. Han, Z. Gao and F. Wang, *Acc. Chem. Res.*, 2018, **51**, 2719–2729; (d) G. Yu, K. Jie and F. Huang, *Chem. Rev.*, 2015, **115**, 7240–7303; (e) L.-J. Chen and H.-B. Yang, *Acc. Chem. Res.*, 2018, **51**, 2699–2710; (f) S. S. Babu, V. K. Praveen and A. Ajayaghosh, *Chem. Rev.*, 2014, **114**, 1973–2129; (g) X. Yu, L. Chen, M. Zhang and T. Yi, *Chem. Soc. Rev.*, 2014, **43**, 5346–5371; (h) C. Wang, Z. Wang and X. Zhang, *Acc. Chem. Res.*, 2012, **45**, 608–618; (i) D.-S. Guo and Y. Liu, *Acc. Chem. Res.*, 2014, **47**, 1925–1934; (j) H. Yang, B. Yuan, X. Zhang and O. A. Scherman, *Acc. Chem. Res.*, 2014, **47**, 2106–2115; (k) P. Xing and Y. Zhao, *Small, Methods*, 2018, **2**, 1700364.
- (a) L. Takacs, *Chem. Soc. Rev.*, 2013, **42**, 7649–7659; (b) A. L. Black, J. M. Lenhardt and S. L. Craig, *J. Mater. Chem.*, 2011, **21**, 1655–1663; (c) T. Matsuda, R. Kawakami, R. Namba, T. Nakajima and J. P. Gong, *Science*, 2019, **363**, 504–508; (d) Y. Yuan, W. Yuan and Y. Chen, *Sci. China Mater.*, 2016, **59**, 507–520; (e) P. Xue, J. Ding, P. Wang and R. Lu, *J. Mater. Chem. C*, 2016, **4**, 6688–6706.
- (a) J. B. Weaver, *Nat. Nanotechnol.*, 2010, **5**, 630–631; (b) T. Qin, B. Liu, K. Zhu, Z. Luo, Y. Huang, C. Pan and L. Wang, *Trends Anal. Chem.*, 2018, **102**, 259–271; (c) X. Wang, O. S. Wolfbeis and R. J. Meier, *Chem. Soc. Rev.*, 2013, **42**, 7834–7869.
- (a) M.-L. He, S. Wu, J. He, Z. Abliz and L. Xu, *RSC Adv.*, 2014, **4**, 2605–2608; (b) X. Yao, X. Ma and H. Tian, *J. Mater. Chem. C*, 2014, **2**, 5155–5160.
- J. Xiong, K. Wang, Z. Yao, B. Zou, J. Xu and X.-H. Bu, *ACS Appl. Mater. Interfaces*, 2018, **10**, 5819–5827.
- (a) B. Yoon, J. Lee, I. S. Park, S. Jeon, J. Lee and J.-M. Kim, *J. Mater. Chem. C*, 2013, **1**, 2388–2403; (b) M. I. Khazi, W. Jeong and J.-M. Kim, *Adv. Mater.*, 2018, **30**, 1705310; (c) L. Chen, J.-W. Ye, H.-P. Wang, M. Pan, S.-Y. Yin, Z.-W. Wei, L.-Y. Zhang, K. Wu, Y.-N. Fan and C.-Y. Su, *Nat. Commun.*, 2017, **8**, 15985; (d) Q. Lin, T.-T. Lu, X. Zhu, T.-B. Wei, H. Li and Y.-M. Zhang, *Chem. Sci.*, 2016, **7**, 5341–5346; (e) J. Wang, C.-F. Wang and S. Chen, *Angew. Chem., Int. Ed.*, 2012, **51**, 9297–9301; (f) Z. An, C. Zheng, Y. Tao, R. Chen, H. Shi, T. Chen, Z. Wang, H. Li, R. Deng, X. Liu and W. Huang, *Nat. Mater.*, 2015, **14**, 685–690; (g) C. Zhang, B. Wang, W. Li, S. Huang, L. Kong, Z. Li and L. Li, *Nat. Commun.*, 2017, **8**, 11386; (h) J. Wei, X. Jiao, T. Wang and D. Chen, *ACS Appl. Mater. Interfaces*, 2016, **8**, 29713–29720; (i) W. Wang, J. Feng, Y. Ye, F. Lyu, Y.-S. Liu, J. Guo and Y. Yin, *Nano Lett.*, 2017, **17**, 755–761; (j) W. Wang, N. Xie, L. He and Y. Yin, *Nat. Commun.*, 2014, **5**, 5459; (k) M. Zuo, W. Qian, T. Li, X.-Y. Hu, J. Jiang and L. Wang, *ACS Appl. Mater. Interfaces*, 2018, **10**, 39214–39221; (l) D. Han, B. Jiang, J. Feng, Y. Yin and W. Wang, *Angew. Chem., Int. Ed.*, 2017, **56**, 7792–7796.
- (a) J.-X. Wang, L.-Y. Niu, P.-Z. Chen, Y.-Z. Chen, Q.-Z. Yang and R. Boulatov, *Chem. Commun.*, 2019, **55**, 7017–7020; (b) Z. Li, G. Wang, Y. Wang and H. Li, *Angew. Chem., Int. Ed.*, 2018, **57**, 2194–2198; (c) Y. Ni, Z. Sun, Y. Wang, H. F. Nour, A. C.-H. Sue, N. S. Finney, K. K. Baldrige and M. A. Olson, *J. Mater. Chem. C*, 2019, **7**, 7399–7410.
- (a) X. Hou, C. Ke, C. J. Bruns, P. R. McGonigal, R. B. Pettman and J. F. Stoddart, *Nat. Commun.*, 2015, **6**, 6884; (b) C.-W. Zhang, B. Ou, S.-T. Jiang, G.-Q. Yin, L.-J. Chen, L. Xu, X. Li and H.-B. Yang, *Polym. Chem.*, 2018, **9**, 2021–2030.
- Z. Wei, Z.-Y. Gu, R. K. Arvapally, Y.-P. Chen, R. N. McDougald, J. F. Ivy, A. A. Yakovenko, D. Feng, M. A. Omary and H.-C. Zhou, *J. Am. Chem. Soc.*, 2014, **136**, 8269–8276.
- (a) H. Chen and Y. Zhao, *ACS Appl. Mater. Interfaces*, 2018, **10**, 21021–21034; (b) P. Xing, H. Chen, H. Xiang and Y. Zhao, *Adv. Mater.*, 2018, **30**, 1705633; (c) L. Zhu, H. Tran, F. L. Beyer, S. D. Walck, X. Li, H. Ågren, K. L. Killops and L. M. Campos, *J. Am. Chem. Soc.*, 2014, **136**, 13381–13387; (d) Z. Gao, Y. Han and F. Wang, *Nat. Commun.*, 2018, **9**, 3977; (e) L. Li, J. M. Scheiger and P. A. Levkin, *Adv. Mater.*, 2019, **31**, 1807333.
- L. Cheng, C. Wang, L. Feng, K. Yang and Z. Liu, *Chem. Rev.*, 2014, **114**, 10869–10939.
- (a) V. Ramamurthy and J. Sivaguru, *Chem. Rev.*, 2016, **116**, 9914–9993; (b) Z.-A. Huang, C. Chen, X.-D. Yang, X.-B. Fan, W. Zhou, C.-H. Tung, L.-Z. Wu and H. Cong, *J. Am. Chem. Soc.*, 2016, **138**, 11144–11147.
- (a) S. Ghorai, J. C. Sumrak, K. M. Hutchins, D.-K. Bučar, A. V. Tivanski and L. R. MacGillivray, *Chem. Sci.*, 2013, **4**, 4304–4308; (b) I. G. Georgiev and L. R. MacGillivray, *Chem. Soc. Rev.*, 2007, **36**, 1239–1248.
- (a) F. Camerel, L. Bonardi, M. Schmutz and R. Ziessel, *J. Am. Chem. Soc.*, 2006, **128**, 4548–4549; (b) G. Venkataramana and S. Sankararaman, *Org. Lett.*, 2006, **8**, 2739–2742; (c) B. Gole, W. Song, M. Lackinger and P. S. Mukherjee, *Chem. – Eur. J.*, 2014, **20**, 13662–13680; (d) Y. Imai, Y. Nakano, T. Kawai and J. Yuasa, *Angew. Chem., Int. Ed.*, 2018, **57**, 8973–8978; (e) Y. Wang, X. Li, F. Li, W.-Y. Sun, C. Zhu and Y. Cheng, *Chem. Commun.*, 2017, **53**, 7505–7508.
- (a) H. Frisch, J. P. Menzel, F. R. Bloesser, D. E. Marschner, K. Mundsinger and C. Barner-Kowollik, *J. Am. Chem. Soc.*, 2018, **140**, 9551–9557; (b) E. Cariati, C. Botta, S. G. Danelli, A. Forni, A. Giaretta, U. Giovanelli, E. Lucenti, D. Marinotto, S. Righetto and R. Ugo, *Chem. Commun.*, 2014, **50**, 14225–14228; (c) P.-P. He, X.-D. Li, L. Wang and H. Wang, *Acc. Chem. Res.*, 2019, **52**, 367–378; (d) K. Murayama, Y. Yamano and

- H. Asanuma, *J. Am. Chem. Soc.*, 2019, **141**, 9485–9489; (e) X. Chang, Z. Zhou, C. Shang, G. Wang, Z. Wang, Y. Qi, Z.-Y. Li, H. Wang, L. Cao, X. Li, Y. Fang and P. J. Stang, *J. Am. Chem. Soc.*, 2019, **141**, 1757–1765.
- 16 K. M. Chan, D. K. Kçlmeç, S. Wang and E. T. Kool, *Angew. Chem., Int. Ed.*, 2017, **56**, 6497–6501.
- 17 S.-X. Tang, N. Wang, X.-D. Xu and S. Feng, *New J. Chem.*, 2019, **43**, 6461–6464.
- 18 (a) X.-D. Xu, C.-J. Yao, L.-J. Chen, G.-Q. Yin, Y.-W. Zhong and H.-B. Yang, *Chem. – Eur. J.*, 2016, **22**, 5211–5218; (b) X.-D. Xu, X. Li, H. Chen, Q. Qu, L. Zhao, H. Ågren and Y. Zhao, *Small*, 2015, **11**, 5901–5906; (c) X.-D. Xu, L. Zhao, Q. Qu, J.-G. Wang, H. Shi and Y. Zhao, *ACS Appl. Mater. Interfaces*, 2015, **7**, 17371–17380; (d) Y. Zuo, H. Lu, L. Xue, X. Wang, L. Ning and S. Feng, *J. Mater. Chem. C*, 2014, **2**, 2724–2734; (e) X.-D. Xu, J. Zhang, L.-J. Chen, R. Guo, D.-X. Wang and H.-B. Yang, *Chem. Commun.*, 2012, **48**, 11223–11225; (f) X.-D. Xu, J. Zhang, X. Yu, L.-J. Chen, D.-X. Wang, T. Yi, F. Li and H.-B. Yang, *Chem. – Eur. J.*, 2012, **18**, 16000–16013; (g) X.-D. Xu, J. Zhang, L.-J. Chen, X.-L. Zhao, D.-X. Wang and H.-B. Yang, *Chem. – Eur. J.*, 2012, **18**, 1659–1667.
- 19 (a) S. Sengupta and F. Würthner, *Chem. Commun.*, 2012, **48**, 5730–5732; (b) Y. Li, X. Li, Y. Li, H. Liu, S. Wang, H. Gan, J. Li, N. Wang, X. He and D. Zhu, *Angew. Chem., Int. Ed.*, 2006, **45**, 3639–3643.
- 20 D. Ke, C. Zhan, A. D. Q. Li and J. Yao, *Angew. Chem., Int. Ed.*, 2011, **50**, 3715–3719.
- 21 M.-M. Gan, J.-Q. Liu, L. Zhang, Y.-Y. Wang, F. E. Hahn and Y.-F. Han, *Chem. Rev.*, 2018, **118**, 9587–9641.
- 22 E. Shi, Z. Gao, M. Yuan, X. Wang and F. Wang, *Polym. Chem.*, 2015, **6**, 5575–5579.
- 23 (a) M. You, M. Lin, S. Wang, X. Wang, G. Zhang, Y. Hong, Y. Dong, G. Jin and F. Xu, *Nanoscale*, 2016, **8**, 10096–10104; (b) M. You, M. Lin, Y. Gong, S. Wang, A. Li, L. Ji, H. Zhao, K. Ling, T. Wen, Y. Huang, D. Gao, Q. Ma, T. Wang, A. Ma, X. Li and F. Xu, *ACS Nano*, 2017, **11**, 6261–6270.